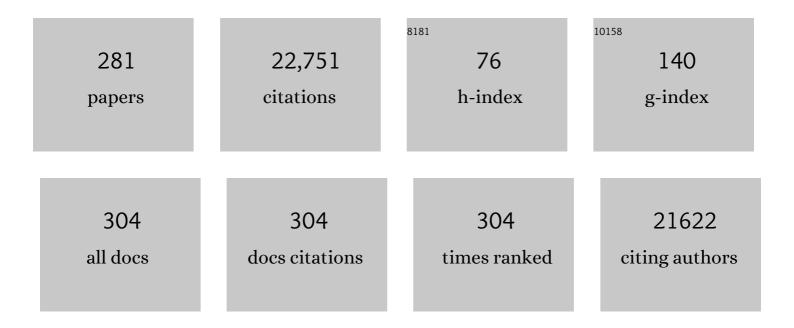
## Ji-Xin Cheng

List of Publications by Year in descending order

Source: https://exaly.com/author-pdf/5080376/publications.pdf Version: 2024-02-01



II-XIN CHENC

#	Article	IF	CITATIONS
1	In vitro and in vivo two-photon luminescence imaging of single gold nanorods. Proceedings of the National Academy of Sciences of the United States of America, 2005, 102, 15752-15756.	7.1	919
2	Coherent Anti-Stokes Raman Scattering Microscopy:  Instrumentation, Theory, and Applications. Journal of Physical Chemistry B, 2004, 108, 827-840.	2.6	897
3	Cholesteryl Ester Accumulation Induced by PTEN Loss and PI3K/AKT Activation Underlies Human Prostate Cancer Aggressiveness. Cell Metabolism, 2014, 19, 393-406.	16.2	671
4	Triacylglycerol Synthesis Enzymes Mediate Lipid Droplet Growth by Relocalizing from the ER to Lipid Droplets. Developmental Cell, 2013, 24, 384-399.	7.0	623
5	Vibrational spectroscopic imaging of living systems: An emerging platform for biology and medicine. Science, 2015, 350, aaa8870.	12.6	599
6	Gold Nanorods Mediate Tumor Cell Death by Compromising Membrane Integrity. Advanced Materials, 2007, 19, 3136-3141.	21.0	545
7	Hyperthermic effects of gold nanorods on tumor cells. Nanomedicine, 2007, 2, 125-132.	3.3	512
8	Gold Nanorods as Contrast Agents for Biological Imaging: Optical Properties, Surface Conjugation and Photothermal Effects <sup>â€</sup> . Photochemistry and Photobiology, 2009, 85, 21-32.	2.5	502
9	Overcoming the barriers in micellar drug delivery: loading efficiency, <i>in vivo</i> stability, and micelle–cell interaction. Expert Opinion on Drug Delivery, 2010, 7, 49-62.	5.0	487
10	Lipid Desaturation Is a Metabolic Marker and Therapeutic Target of Ovarian Cancer Stem Cells. Cell Stem Cell, 2017, 20, 303-314.e5.	11.1	414
11	Laser-Scanning Coherent Anti-Stokes Raman Scattering Microscopy and Applications to Cell Biology. Biophysical Journal, 2002, 83, 502-509.	0.5	378
12	Release of hydrophobic molecules from polymer micelles into cell membranes revealed by Förster resonance energy transfer imaging. Proceedings of the National Academy of Sciences of the United States of America, 2008, 105, 6596-6601.	7.1	358
13	Polarization coherent anti-Stokes Raman scattering microscopy. Optics Letters, 2001, 26, 1341.	3.3	354
14	Theoretical and experimental characterization of coherent anti-Stokes Raman scattering microscopy. Journal of the Optical Society of America B: Optical Physics, 2002, 19, 1363.	2.1	332
15	Multiplex Coherent Anti-Stokes Raman Scattering Microspectroscopy and Study of Lipid Vesicles. Journal of Physical Chemistry B, 2002, 106, 8493-8498.	2.6	324
16	An Epi-Detected Coherent Anti-Stokes Raman Scattering (E-CARS) Microscope with High Spectral Resolution and High Sensitivity. Journal of Physical Chemistry B, 2001, 105, 1277-1280.	2.6	319
17	Vibrational Imaging with High Sensitivity via Epidetected Coherent Anti-Stokes Raman Scattering Microscopy. Physical Review Letters, 2001, 87, .	7.8	299
18	Coherent Anti-Stokes Raman Scattering Imaging of Axonal Myelin in Live Spinal Tissues. Biophysical Journal, 2005, 89, 581-591.	0.5	295

#	Article	IF	CITATIONS
19	Fast Release of Lipophilic Agents from Circulating PEG-PDLLA Micelles Revealed by <i>in Vivo</i> F¶rster Resonance Energy Transfer Imaging. Langmuir, 2008, 24, 5213-5217.	3.5	293
20	Controlling the Cellular Uptake of Gold Nanorods. Langmuir, 2007, 23, 1596-1599.	3.5	288
21	Vibrational imaging of lipid droplets in live fibroblast cells with coherent anti-Stokes Raman scattering microscopy. Journal of Lipid Research, 2003, 44, 2202-2208.	4.2	275
22	Single Cell Optical Imaging and Spectroscopy. Chemical Reviews, 2013, 113, 2469-2527.	47.7	250
23	Depth-resolved mid-infrared photothermal imaging of living cells and organisms with submicrometer spatial resolution. Science Advances, 2016, 2, e1600521.	10.3	229
24	A Comparative Study of Fat Storage Quantitation in Nematode Caenorhabditis elegans Using Label and Label-Free Methods. PLoS ONE, 2010, 5, e12810.	2.5	202
25	Ordering of water molecules between phospholipid bilayers visualized by coherent anti-Stokes Raman scattering microscopy. Proceedings of the National Academy of Sciences of the United States of America, 2003, 100, 9826-9830.	7.1	198
26	Quantitative Vibrational Imaging by Hyperspectral Stimulated Raman Scattering Microscopy and Multivariate Curve Resolution Analysis. Analytical Chemistry, 2013, 85, 98-106.	6.5	198
27	Characterization of photodamage in coherent anti-Stokes Raman scattering microscopy. Optics Express, 2006, 14, 3942.	3.4	182
28	Microsecond scale vibrational spectroscopic imaging by multiplex stimulated Raman scattering microscopy. Light: Science and Applications, 2015, 4, e265-e265.	16.6	172
29	All-Glass, Large Metalens at Visible Wavelength Using Deep-Ultraviolet Projection Lithography. Nano Letters, 2019, 19, 8673-8682.	9.1	165
30	Green's function formulation for third-harmonic generation microscopy. Journal of the Optical Society of America B: Optical Physics, 2002, 19, 1604.	2.1	162
31	Coherent anti-Stokes Raman scattering imaging of lipids in cancer metastasis. BMC Cancer, 2009, 9, 42.	2.6	156
32	Coherent Raman Scattering Microscopy in Biology and Medicine. Annual Review of Biomedical Engineering, 2015, 17, 415-445.	12.3	153
33	Ex vivo and in vivo imaging of myelin fibers in mouse brain by coherent anti-Stokes Raman scattering microscopy. Optics Express, 2008, 16, 19396.	3.4	151
34	Label-free molecular imaging of atherosclerotic lesions using multimodal nonlinear optical microscopy. Journal of Biomedical Optics, 2007, 12, 054007.	2.6	146
35	Shedding new light on lipid biology with coherent anti-Stokes Raman scattering microscopy. Journal of Lipid Research, 2010, 51, 3091-3102.	4.2	142
36	Highly Sensitive Vibrational Imaging by Femtosecond Pulse Stimulated Raman Loss. Journal of Physical Chemistry Letters, 2011, 2, 1248-1253.	4.6	142

#	Article	IF	CITATIONS
37	Meta-optics achieves RGB-achromatic focusing for virtual reality. Science Advances, 2021, 7, .	10.3	142
38	Multimodal nonlinear optical microscopy. Laser and Photonics Reviews, 2011, 5, 496-512.	8.7	139
39	Direct Visualization of De novo Lipogenesis in Single Living Cells. Scientific Reports, 2014, 4, 6807.	3.3	139
40	Semiconducting Polymer Nanoparticles for Centimetersâ€Deep Photoacoustic Imaging in the Second Nearâ€Infrared Window. Advanced Materials, 2017, 29, 1703403.	21.0	136
41	Curcumin inhibits adipocyte differentiation through modulation of mitotic clonal expansion. Journal of Nutritional Biochemistry, 2011, 22, 910-920.	4.2	134
42	Fast Vibrational Imaging of Single Cells and Tissues by Stimulated Raman Scattering Microscopy. Accounts of Chemical Research, 2014, 47, 2282-2290.	15.6	134
43	Bright Threeâ€Photon Luminescence from Gold/Silver Alloyed Nanostructures for Bioimaging with Negligible Photothermal Toxicity. Angewandte Chemie - International Edition, 2010, 49, 3485-3488.	13.8	133
44	High-Quality Manganese-Doped Zinc Sulfide Quantum Rods with Tunable Dual-Color and Multiphoton Emissions. Journal of the American Chemical Society, 2011, 133, 5389-5396.	13.7	132
45	Label-Free Bond-Selective Imaging by Listening to Vibrationally Excited Molecules. Physical Review Letters, 2011, 106, 238106.	7.8	132
46	Far-field imaging of non-fluorescent species with subdiffraction resolution. Nature Photonics, 2013, 7, 449-453.	31.4	131
47	High-Speed Vibrational Imaging and Spectral Analysis of Lipid Bodies by Compound Raman Microscopy. Journal of Physical Chemistry B, 2009, 113, 7681-7686.	2.6	126
48	A multimodal platform for nonlinear optical microscopy and microspectroscopy. Optics Express, 2009, 17, 1282.	3.4	126
49	Coherent Anti-Stokes Raman Scattering Microscopy. Applied Spectroscopy, 2007, 61, 197A-208A.	2.2	124
50	Label-free imaging of arterial cells and extracellular matrix using a multimodal CARS microscope. Optics Communications, 2008, 281, 1813-1822.	2.1	122
51	A dynamic, cytoplasmic triacylglycerol pool in enterocytes revealed by ex vivo and in vivo coherent anti-Stokes Raman scattering imaging. Journal of Lipid Research, 2009, 50, 1080-1089.	4.2	122
52	Assessing Cholesterol Storage in Live Cells and C. elegans by Stimulated Raman Scattering Imaging of Phenyl-Diyne Cholesterol. Scientific Reports, 2015, 5, 7930.	3.3	122
53	Quantitative Coherent Anti-Stokes Raman Scattering Imaging of Lipid Distribution in Coexisting Domains. Biophysical Journal, 2005, 89, 3480-3490.	0.5	120
54	Frizzled-7 Identifies Platinum-Tolerant Ovarian Cancer Cells Susceptible to Ferroptosis. Cancer Research, 2021, 81, 384-399.	0.9	113

#	Article	IF	CITATIONS
55	Selective Detection of Protein Crystals by Second Harmonic Microscopy. Journal of the American Chemical Society, 2008, 130, 14076-14077.	13.7	109
56	High-speed Intravascular Photoacoustic Imaging of Lipid-laden Atherosclerotic Plaque Enabled by a 2-kHz Barium Nitrite Raman Laser. Scientific Reports, 2014, 4, 6889.	3.3	107
57	Neuroprotective ferulic acid (FA)–glycol chitosan (GC) nanoparticles for functional restoration of traumatically injured spinal cord. Biomaterials, 2014, 35, 2355-2364.	11.4	105
58	Coherent anti-stokes Raman scattering imaging of myelin degradation reveals a calcium-dependent pathway in lyso-PtdCho-induced demyelination. Journal of Neuroscience Research, 2007, 85, 2870-2881.	2.9	103
59	Effective repair of traumatically injured spinal cord by nanoscale block copolymer micelles. Nature Nanotechnology, 2010, 5, 80-87.	31.5	102
60	Blood-stable, tumor-adaptable disulfide bonded mPEG-(Cys)4-PDLLA micelles for chemotherapy. Biomaterials, 2013, 34, 552-561.	11.4	102
61	Assessing breast tumor margin by multispectral photoacoustic tomography. Biomedical Optics Express, 2015, 6, 1273.	2.9	101
62	Imaging and Quantitative Analysis of Atherosclerotic Lesions by CARS-Based Multimodal Nonlinear Optical Microscopy. Arteriosclerosis, Thrombosis, and Vascular Biology, 2009, 29, 1342-1348.	2.4	99
63	Label-free quantitative analysis of lipid metabolism in living Caenorhabditis elegans. Journal of Lipid Research, 2010, 51, 672-677.	4.2	99
64	Spectrally modulated stimulated Raman scattering imaging with an angle-to-wavelength pulse shaper. Optics Express, 2013, 21, 13864.	3.4	98
65	Nrg4 promotes fuel oxidation and a healthy adipokine profile to ameliorate diet-induced metabolic disorders. Molecular Metabolism, 2017, 6, 863-872.	6.5	97
66	Actionable Cytopathogenic Host Responses of Human Alveolar Type 2 Cells to SARS-CoV-2. Molecular Cell, 2020, 80, 1104-1122.e9.	9.7	94
67	Label-free imaging of semiconducting and metallic carbon nanotubes in cells and mice using transient absorption microscopy. Nature Nanotechnology, 2012, 7, 56-61.	31.5	93
68	Vibrational imaging of tablets by epi-detected stimulated Raman scattering microscopy. Analyst, The, 2010, 135, 2613.	3.5	91
69	Labelâ€Free Quantitative Imaging of Cholesterol in Intact Tissues by Hyperspectral Stimulated Raman Scattering Microscopy. Angewandte Chemie - International Edition, 2013, 52, 13042-13046.	13.8	91
70	Ultrafast chemical imaging by widefield photothermal sensing of infrared absorption. Science Advances, 2019, 5, eaav7127.	10.3	89
71	Spectrometer-free vibrational imaging by retrieving stimulated Raman signal from highly scattered photons. Science Advances, 2015, 1, e1500738.	10.3	88
72	Second Harmonic and Sum Frequency Generation Imaging of Fibrous Astroglial Filaments in Ex Vivo Spinal Tissues. Biophysical Journal, 2007, 92, 3251-3259.	0.5	87

#	Article	IF	CITATIONS
73	Plk1 Inhibition Enhances the Efficacy of Androgen Signaling Blockade in Castration-Resistant Prostate Cancer. Cancer Research, 2014, 74, 6635-6647.	0.9	87
74	Glutamate Excitotoxicity Inflicts Paranodal Myelin Splitting and Retraction. PLoS ONE, 2009, 4, e6705.	2.5	86
75	Stimulated Raman scattering flow cytometry for label-free single-particle analysis. Optica, 2017, 4, 103.	9.3	86
76	Antibiotic Susceptibility Determination within One Cell Cycle at Single-Bacterium Level by Stimulated Raman Metabolic Imaging. Analytical Chemistry, 2018, 90, 3737-3743.	6.5	86
77	Interaction of tau with HNRNPA2B1 and N6-methyladenosine RNA mediates the progression of tauopathy. Molecular Cell, 2021, 81, 4209-4227.e12.	9.7	84
78	Photochemical Tagging for Quantitation of Unsaturated Fatty Acids by Mass Spectrometry. Analytical Chemistry, 2016, 88, 8931-8935.	6.5	82
79	Imaging Lipid Metabolism in Live <i>Caenorhabditis elegans</i> Using Fingerprint Vibrations. Angewandte Chemie - International Edition, 2014, 53, 11787-11792.	13.8	78
80	High-sensitivity intravascular photoacoustic imaging of lipid–laden plaque with a collinear catheter design. Scientific Reports, 2016, 6, 25236.	3.3	78
81	Plasmon-enhanced stimulated Raman scattering microscopy with single-molecule detection sensitivity. Nature Communications, 2019, 10, 5318.	12.8	77
82	Differential association of adipophilin and TIP47 proteins with cytoplasmic lipid droplets in mouse enterocytes during dietary fat absorption. Biochimica Et Biophysica Acta - Molecular and Cell Biology of Lipids, 2009, 1791, 1173-1180.	2.4	74
83	The Layered Structure of Coronary Adventitia under Mechanical Load. Biophysical Journal, 2011, 101, 2555-2562.	0.5	74
84	Bondâ€selective imaging of deep tissue through the optical window between 1600 and 1850 nm. Journal of Biophotonics, 2012, 5, 25-32.	2.3	74
85	Stimulated Raman spectroscopic imaging by microsecond delay-line tuning. Optica, 2016, 3, 1377.	9.3	73
86	Synchronization of two passively mode-locked, picosecond lasers within 20 fs for coherent anti-Stokes Raman scattering microscopy. Review of Scientific Instruments, 2002, 73, 2843-2848.	1.3	72
87	Intestine-specific expression of acyl CoA:diacylglycerol acyltransferase 1 reverses resistance to diet-induced hepatic steatosis and obesity in Dgat1 mice. Journal of Lipid Research, 2010, 51, 1770-1780.	4.2	72
88	Rapid Determination of Antimicrobial Susceptibility by Stimulated Raman Scattering Imaging of D <sub>2</sub> 0 Metabolic Incorporation in a Single Bacterium. Advanced Science, 2020, 7, 2001452.	11.2	72
89	Multiplex Stimulated Raman Scattering Imaging Cytometry Reveals Lipid-Rich Protrusions in Cancer Cells under Stress Condition. IScience, 2020, 23, 100953.	4.1	72
90	Compression Induces Acute Demyelination and Potassium Channel Exposure in Spinal Cord. Journal of Neurotrauma, 2010, 27, 1109-1120.	3.4	70

#	Article	IF	CITATIONS
91	Perspective: Coherent Raman scattering microscopy, the future is bright. APL Photonics, 2018, 3, .	5.7	69
92	Avasimibe Encapsulated in Human Serum Albumin Blocks Cholesterol Esterification for Selective Cancer Treatment. ACS Nano, 2015, 9, 2420-2432.	14.6	68
93	Mid-Infrared Photothermal Imaging of Active Pharmaceutical Ingredients at Submicrometer Spatial Resolution. Analytical Chemistry, 2017, 89, 4863-4867.	6.5	68
94	Real-time intravascular photoacoustic-ultrasound imaging of lipid-laden plaque in human coronary artery at 16 frames per second. Scientific Reports, 2017, 7, 1417.	3.3	68
95	In Situ Visualization of Paclitaxel Distribution and Release by Coherent Anti-Stokes Raman Scattering Microscopy. Analytical Chemistry, 2006, 78, 8036-8043.	6.5	67
96	Bond-selective photoacoustic imaging by converting molecular vibration into acoustic waves. Photoacoustics, 2016, 4, 11-21.	7.8	66
97	Microfluidic CARS cytometry. Optics Express, 2008, 16, 5782.	3.4	63
98	Heterodyne detected nonlinear optical imaging in a lockâ€in free manner. Journal of Biophotonics, 2012, 5, 801-807.	2.3	63
99	Nanomedicine for treating spinal cord injury. Nanoscale, 2013, 5, 8821.	5.6	63
100	Quantification of Lipid Metabolism in Living Cells through the Dynamics of Lipid Droplets Measured by Stimulated Raman Scattering Imaging. Analytical Chemistry, 2017, 89, 4502-4507.	6.5	63
101	Bond-selective transient phase imaging via sensing of the infrared photothermal effect. Light: Science and Applications, 2019, 8, 116.	16.6	62
102	Volumetric chemical imaging by stimulated Raman projection microscopy and tomography. Nature Communications, 2017, 8, 15117.	12.8	61
103	Bond-selective imaging by optically sensing the mid-infrared photothermal effect. Science Advances, 2021, 7, .	10.3	61
104	In Vitro and In Vivo Nonlinear Optical Imaging of Silicon Nanowires. Nano Letters, 2009, 9, 2440-2444.	9.1	60
105	Paclitaxel distribution in poly(ethylene glycol)/poly(lactide-co-glycolic acid) blends and its release visualized by coherent anti-Stokes Raman scattering microscopy. Journal of Controlled Release, 2007, 122, 261-268.	9.9	59
106	Photolysis of Staphyloxanthin in Methicillinâ€Resistant <i>Staphylococcus aureus</i> Potentiates Killing by Reactive Oxygen Species. Advanced Science, 2019, 6, 1900030.	11.2	59
107	<i>In Vivo</i> and <i>in Situ</i> Spectroscopic Imaging by a Handheld Stimulated Raman Scattering Microscope. ACS Photonics, 2018, 5, 947-954.	6.6	58
108	Microsecond fingerprint stimulated Raman spectroscopic imaging by ultrafast tuning and spatial-spectral learning. Nature Communications, 2021, 12, 3052.	12.8	58

#	Article	IF	CITATIONS
109	Biaxial deformation of collagen and elastin fibers in coronary adventitia. Journal of Applied Physiology, 2013, 115, 1683-1693.	2.5	57
110	Raman microspectroscopy for microbiology. Nature Reviews Methods Primers, 2021, 1, .	21.2	57
111	Deciphering single cell metabolism by coherent Raman scattering microscopy. Current Opinion in Chemical Biology, 2016, 33, 46-57.	6.1	55
112	Fingerprinting a Living Cell by Raman Integrated Mid-Infrared Photothermal Microscopy. Analytical Chemistry, 2019, 91, 10750-10756.	6.5	55
113	Molecular Composition and Orientation in Myelin Figures Characterized by Coherent Anti-Stokes Raman Scattering Microscopy. Langmuir, 2005, 21, 6478-6486.	3.5	54
114	Gold nanorod-mediated photothermolysis induces apoptosis of macrophages via damage of mitochondria. Nanomedicine, 2009, 4, 265-276.	3.3	54
115	Longitudinal in vivo coherent anti-Stokes Raman scattering imaging of demyelination and remyelination in injured spinal cord. Journal of Biomedical Optics, 2011, 16, 1.	2.6	54
116	Multimodal Nonlinear Optical Microscopy and Applications to Central Nervous System Imaging. IEEE Journal of Selected Topics in Quantum Electronics, 2008, 14, 4-9.	2.9	53
117	High-speed stimulated hyperspectral Raman imaging using rapid acousto-optic delay lines. Optics Letters, 2017, 42, 1548.	3.3	53
118	Label-Free Imaging of Lipid-Droplet Intracellular Motion in Early Drosophila Embryos Using Femtosecond-Stimulated Raman Loss Microscopy. Biophysical Journal, 2012, 102, 1666-1675.	0.5	52
119	Fast assessment of lipid content in arteries in vivo by intravascular photoacoustic tomography. Scientific Reports, 2018, 8, 2400.	3.3	52
120	Cholesterol Esterification Inhibition Suppresses Prostate Cancer Metastasis by Impairing the Wnt/β-catenin Pathway. Molecular Cancer Research, 2018, 16, 974-985.	3.4	52
121	Single-Cell Profiling Reveals the Origin of Phenotypic Variability in Adipogenesis. PLoS ONE, 2009, 4, e5189.	2.5	51
122	Mapping lipid and collagen by multispectral photoacoustic imaging of chemical bond vibration. Journal of Biomedical Optics, 2012, 17, 0960101.	2.6	51
123	Spectroscopic stimulated Raman scattering imaging of highly dynamic specimens through matrix completion. Light: Science and Applications, 2018, 7, 17179-17179.	16.6	51
124	Real-Time CARS Imaging Reveals a Calpain-Dependent Pathway for Paranodal Myelin Retraction during High-Frequency Stimulation. PLoS ONE, 2011, 6, e17176.	2.5	51
125	Acrolein induces myelin damage in mammalian spinal cord. Journal of Neurochemistry, 2011, 117, 554-564.	3.9	50
126	Paranodal myelin retraction in relapsing experimental autoimmune encephalomyelitis visualized by coherent anti-Stokes Raman scattering microscopy. Journal of Biomedical Optics, 2011, 16, 106006.	2.6	49

#	Article	IF	CITATIONS
127	Spectroscopic Imaging of Deep Tissue through Photoacoustic Detection of Molecular Vibration. Journal of Physical Chemistry Letters, 2013, 4, 2177-2185.	4.6	49
128	Bond-Selective Imaging of Cells by Mid-Infrared Photothermal Microscopy in High Wavenumber Region. Journal of Physical Chemistry B, 2017, 121, 10249-10255.	2.6	49
129	Nonlinear Optical Imaging to Evaluate the Impact of Obesity on Mammary Gland and Tumor Stroma. Molecular Imaging, 2007, 6, 7290.2007.00018.	1.4	48
130	Chasing lipids in health and diseases by coherent anti-Stokes Raman scattering microscopy. Vibrational Spectroscopy, 2009, 50, 160-167.	2.2	48
131	Label-Free Vibrational Spectroscopic Imaging of Neuronal Membrane Potential. Journal of Physical Chemistry Letters, 2017, 8, 1932-1936.	4.6	48
132	Visualizing Systemic Clearance and Cellular Level Biodistribution of Gold Nanorods by Intrinsic Two-Photon Luminescence. Langmuir, 2009, 25, 12454-12459.	3.5	47
133	FRET Imaging Reveals Different Cellular Entry Routes of Self-Assembled and Disulfide Bonded Polymeric Micelles. Molecular Pharmaceutics, 2013, 10, 3497-3506.	4.6	47
134	Optoacoustic brain stimulation at submillimeter spatial precision. Nature Communications, 2020, 11, 881.	12.8	47
135	Fast Detection of the Metallic State of Individual Single-Walled Carbon Nanotubes Using a Transient-Absorption Optical Microscope. Physical Review Letters, 2010, 105, 217401.	7.8	46
136	Label-free imaging through nonlinear optical signals. Materials Today, 2011, 14, 264-273.	14.2	45
137	Label-free spectroscopic detection of membrane potential using stimulated Raman scattering. Applied Physics Letters, 2015, 106, .	3.3	44
138	Cholesterol esterification inhibition and gemcitabine synergistically suppress pancreatic ductal adenocarcinoma proliferation. PLoS ONE, 2018, 13, e0193318.	2.5	43
139	Label-Free Analysis of Breast Tissue Polarity by Raman Imaging of LipidÂPhase. Biophysical Journal, 2012, 102, 1215-1223.	0.5	42
140	Coherent Anti-Stokes Raman Scattering Correlation Spectroscopy:Â Probing Dynamical Processes with Chemical Selectivity. Journal of Physical Chemistry A, 2002, 106, 8561-8568.	2.5	41
141	High-speed intravascular photoacoustic imaging at 17 μm with a KTP-based OPO. Biomedical Optics Express, 2015, 6, 4557.	2.9	41
142	Transient absorption microscopy: Technological innovations and applications in materials science and life science. Journal of Chemical Physics, 2020, 152, 020901.	3.0	41
143	Cholesterol esterification inhibition and imatinib treatment synergistically inhibit growth of BCR-ABL mutation-independent resistant chronic myelogenous leukemia. PLoS ONE, 2017, 12, e0179558.	2.5	41
144	Imaging Gold Nanorods by Plasmon-Resonance-Enhanced Four Wave Mixing. Journal of Physical Chemistry C, 2009, 113, 2657-2663.	3.1	40

#	Article	IF	CITATIONS
145	Novel Potassium Channel Blocker, 4-AP-3-MeOH, Inhibits Fast Potassium Channels and Restores Axonal Conduction in Injured Guinea Pig Spinal Cord White Matter. Journal of Neurophysiology, 2010, 103, 469-478.	1.8	40
146	Imaging chemistry inside living cells by stimulated Raman scattering microscopy. Methods, 2017, 128, 119-128.	3.8	39
147	Nonlinear optical imaging to evaluate the impact of obesity on mammary gland and tumor stroma. Molecular Imaging, 2007, 6, 205-11.	1.4	39
148	Morphological and Biomechanical Differences in the Elastase and AngII <i>apoE</i> <sup><i>â^'â^'</i></sup> Rodent Models of Abdominal Aortic Aneurysms. BioMed Research International, 2015, 2015, 1-12.	1.9	38
149	High-Speed Chemical Imaging by Dense-Net Learning of Femtosecond Stimulated Raman Scattering. Journal of Physical Chemistry Letters, 2020, 11, 8573-8578.	4.6	38
150	Vibrational Spectroscopic Detection of a Single Virus by Mid-Infrared Photothermal Microscopy. Analytical Chemistry, 2021, 93, 4100-4107.	6.5	37
151	Fluorescence-Detected Mid-Infrared Photothermal Microscopy. Journal of the American Chemical Society, 2021, 143, 11490-11499.	13.7	37
152	Evolution of Membrane Fouling Revealed by Label-Free Vibrational Spectroscopic Imaging. Environmental Science & Technology, 2017, 51, 9580-9587.	10.0	36
153	Volumetric stimulated Raman scattering imaging of cleared tissues towards three-dimensional chemical histopathology. Biomedical Optics Express, 2019, 10, 4329.	2.9	36
154	Nonlinear Optical Microscopy of Single Nanostructures. Annual Review of Materials Research, 2013, 43, 213-236.	9.3	35
155	In Situ and In Vivo Molecular Analysis by Coherent Raman Scattering Microscopy. Annual Review of Analytical Chemistry, 2016, 9, 69-93.	5.4	35
156	Paranodal Myelin Damage after Acute Stretch in Guinea Pig Spinal Cord. Journal of Neurotrauma, 2012, 29, 611-619.	3.4	34
157	Denoising Stimulated Raman Spectroscopic Images by Total Variation Minimization. Journal of Physical Chemistry C, 2015, 119, 19397-19403.	3.1	34
158	Photoâ€Disassembly of Membrane Microdomains Revives Conventional Antibiotics against MRSA. Advanced Science, 2020, 7, 1903117.	11.2	34
159	Functionalized NIRâ€II Semiconducting Polymer Nanoparticles for Singleâ€cell to Wholeâ€Organ Imaging of PSMAâ€Positive Prostate Cancer. Small, 2020, 16, e2001215.	10.0	34
160	Two-photon luminescence imaging of Bacillus spores using peptide-functionalized gold nanorods. Nano Research, 2008, 1, 450-456.	10.4	32
161	Vibrational Fingerprint Mapping Reveals Spatial Distribution of Functional Groups of Lignin in Plant Cell Wall. Analytical Chemistry, 2015, 87, 9436-9442.	6.5	32
162	Neural Stimulation InÂVitro and InÂVivo by Photoacoustic Nanotransducers. Matter, 2021, 4, 654-674.	10.0	32

#	Article	IF	CITATIONS
163	Unveiling Cancer Metabolism through Spontaneous and Coherent Raman Spectroscopy and Stable Isotope Probing. Cancers, 2021, 13, 1718.	3.7	32
164	Multimodal coherent anti-Stokes Raman spectroscopic imaging with a fiber optical parametric oscillator. Applied Physics Letters, 2011, 98, 191106.	3.3	31
165	Quantitative Assessment of Liver Steatosis and Affected Pathways with Molecular Imaging and Proteomic Profiling. Scientific Reports, 2018, 8, 3606.	3.3	31
166	Label-Free Imaging of Heme Dynamics in Living Organisms by Transient Absorption Microscopy. Analytical Chemistry, 2018, 90, 3395-3401.	6.5	31
167	Increasing the imaging depth of coherent anti-Stokes Raman scattering microscopy with a miniature microscope objective. Optics Letters, 2007, 32, 2212.	3.3	30
168	Highly sensitive transient absorption imaging of graphene and graphene oxide in living cells and circulating blood. Scientific Reports, 2015, 5, 12394.	3.3	30
169	Labelâ€free <i>in vivo</i> imaging of peripheral nerve by multispectral photoacoustic tomography. Journal of Biophotonics, 2016, 9, 124-128.	2.3	29
170	3,3'â€Diindolylmethane suppresses highâ€fat dietâ€induced obesity through inhibiting adipogenesis of preâ€adipocytes by targeting USP2 activity. Molecular Nutrition and Food Research, 2017, 61, 1700119.	3.3	29
171	In vitro exploration of ACAT contributions to lipid droplet formation during adipogenesis. Journal of Lipid Research, 2018, 59, 820-829.	4.2	29
172	Imaging Chemical Kinetics of Radical Polymerization with an Ultrafast Coherent Raman Microscope. Advanced Science, 2020, 7, 1903644.	11.2	29
173	Experimental observation and theoretical analysis of Raman resonance-enhanced photodamage in coherent anti-Stokes Raman scattering microscopy. Journal of the Optical Society of America B: Optical Physics, 2007, 24, 544.	2.1	28
174	Spectral analysis assisted photoacoustic imaging for lipid composition differentiation. Photoacoustics, 2017, 7, 12-19.	7.8	28
175	A fiber optoacoustic guide with augmented reality for precision breast-conserving surgery. Light: Science and Applications, 2018, 7, 2.	16.6	28
176	Polarization-sensitive stimulated Raman scattering imaging resolves amphotericin B orientation in <i>Candida</i> membrane. Science Advances, 2021, 7, .	10.3	27
177	Non-genetic photoacoustic stimulation of single neurons by a tapered fiber optoacoustic emitter. Light: Science and Applications, 2021, 10, 143.	16.6	27
178	Nanosecond-resolution photothermal dynamic imaging via MHZ digitization and match filtering. Nature Communications, 2021, 12, 7097.	12.8	27
179	High-Speed Spectroscopic Transient Absorption Imaging of Defects in Graphene. Nano Letters, 2018, 18, 1489-1497.	9.1	26
180	High-resolution photoacoustic endoscope through beam self-cleaning in a graded index fiber. Optics Letters, 2019, 44, 3841.	3.3	26

#	Article	IF	CITATIONS
181	Compact high power barium nitrite crystal-based Raman laser at 1197Ânm for photoacoustic imaging of fat. Journal of Biomedical Optics, 2013, 18, 040502.	2.6	25
182	Stimulated Raman Imaging Reveals Aberrant Lipogenesis as a Metabolic Marker for Azole-Resistant <i>Candida albicans</i> . Analytical Chemistry, 2017, 89, 9822-9829.	6.5	25
183	Fingerprint Stimulated Raman Scattering Imaging Reveals Retinoid Coupling Lipid Metabolism and Survival. ChemPhysChem, 2018, 19, 2500-2506.	2.1	25
184	Label-Free Coherent Anti-Stokes Raman Scattering Imaging of Coexisting Lipid Domains in Single Bilayers. Journal of Physical Chemistry B, 2008, 112, 1576-1579.	2.6	24
185	Label-free quantitation of glycated hemoglobin in single red blood cells by transient absorption microscopy and phasor analysis. Science Advances, 2019, 5, eaav0561.	10.3	24
186	Assessment of White Matter Loss Using Bond-Selective Photoacoustic Imaging in a Rat Model of Contusive Spinal Cord Injury. Journal of Neurotrauma, 2014, 31, 1998-2002.	3.4	23
187	Label-free real-time imaging of myelination in the <i>Xenopus laevis</i> tadpole by <i>in vivo</i> stimulated Raman scattering microscopy. Journal of Biomedical Optics, 2014, 19, 086005.	2.6	23
188	Photoacoustic tomography of intact human prostates and vascular texture analysis identify prostate cancer biopsy targets. Photoacoustics, 2018, 11, 46-55.	7.8	22
189	Dual-wavelength photo-killing of methicillin-resistant Staphylococcus aureus. JCI Insight, 2020, 5, .	5.0	22
190	Quinine Enhances Photo-Inactivation of Gram-Negative Bacteria. Journal of Infectious Diseases, 2020, 221, 618-626.	4.0	21
191	Tau Oligomers and Fibrils Exhibit Differential Patterns of Seeding and Association With RNA Binding Proteins. Frontiers in Neurology, 2020, 11, 579434.	2.4	21
192	Ultrasensitive Vibrational Imaging of Retinoids by Visible Preresonance Stimulated Raman Scattering Microscopy. Advanced Science, 2021, 8, 2003136.	11.2	21
193	siRNA Delivery Using Dithiocarbamate-Anchored Oligonucleotides on Gold Nanorods. Bioconjugate Chemistry, 2019, 30, 443-453.	3.6	20
194	Fingerprinting Bacterial Metabolic Response to Erythromycin by Raman-Integrated Mid-Infrared Photothermal Microscopy. Analytical Chemistry, 2020, 92, 14459-14465.	6.5	20
195	Application of coherent antiâ€stokes Raman scattering microscopy to image the changes in a paclitaxel–poly(styreneâ€ <i>b</i> â€isobutyleneâ€ <i>b</i> â€istyrene) matrix preâ€and postâ€drug elution. Jou of Biomedical Materials Research - Part A, 2008, 87A, 913-920.	urmab	19
196	<i>In situ</i> Detection of a Single Bacterium in Complex Environment by Hyperspectral CARS Imaging. ChemistrySelect, 2016, 1, 513-517.	1.5	19
197	Timeâ€lens based hyperspectral stimulated Raman scattering imaging and quantitative spectral analysis. Journal of Biophotonics, 2013, 6, 815-820.	2.3	18
198	A fiber optoacoustic emitter with controlled ultrasound frequency for cell membrane sonoporation at submillimeter spatial resolution. Photoacoustics, 2020, 20, 100208.	7.8	18

#	Article	IF	CITATIONS
199	Ambient Oxygen-Doped Conjugated Polymer for pH-Activatable Aggregation-Enhanced Photoacoustic Imaging in the Second Near-Infrared Window. Analytical Chemistry, 2021, 93, 3189-3195.	6.5	18
200	Background-Suppressed High-Throughput Mid-Infrared Photothermal Microscopy via Pupil Engineering. ACS Photonics, 2021, 8, 3323-3336.	6.6	18
201	Intermuscular Adipose Tissue Content and Intramyocellular Lipid Fatty Acid Saturation Are Associated with Glucose Homeostasis in Middle-Aged and Older Adults. Endocrinology and Metabolism, 2017, 32, 257.	3.0	17
202	Polymer Electrochromism Driven by Metabolic Activity Facilitates Rapid and Facile Bacterial Detection and Susceptibility Evaluation. Advanced Functional Materials, 2020, 30, 2005192.	14.9	17
203	Staphyloxanthin Photolysis Potentiates Low Concentration Silver Nanoparticles in Eradication of Methicillin-Resistant <i>Staphylococcus aureus</i> . Journal of Physical Chemistry C, 2020, 124, 5321-5330.	3.1	17
204	SRS-FISH: A high-throughput platform linking microbiome metabolism to identity at the single-cell level. Proceedings of the National Academy of Sciences of the United States of America, 2022, 119, .	7.1	17
205	New imaging techniques in the diagnosis of multiple sclerosis. Expert Opinion on Medical Diagnostics, 2008, 2, 1055-1065.	1.6	16
206	Volumetric chemical imaging in vivo by a remote-focusing stimulated Raman scattering microscope. Optics Express, 2020, 28, 30210.	3.4	16
207	Multimodal Metabolic Imaging Reveals Pigment Reduction and Lipid Accumulation in Metastatic Melanoma. BME Frontiers, 2021, 2021, .	4.5	16
208	Imaging growth of neurites in conditioned hydrogel by coherent anti-Stokes Raman scattering microscopy. Organogenesis, 2009, 5, 231-237.	1.2	15
209	Mechanisms of Epi-Detected Stimulated Raman Scattering Microscopy. IEEE Journal of Selected Topics in Quantum Electronics, 2012, 18, 384-388.	2.9	15
210	Vibrational Photoacoustic Tomography: Chemical Imaging beyond the Ballistic Regime. Journal of Physical Chemistry Letters, 2013, 4, 3211-3215.	4.6	15
211	Comparative Quantification of Arterial Lipid by Intravascular Photoacoustic-Ultrasound Imaging and Near-Infrared Spectroscopy-Intravascular Ultrasound. Journal of Cardiovascular Translational Research, 2019, 12, 211-220.	2.4	15
212	Label-free optical imaging of membrane potential. Current Opinion in Biomedical Engineering, 2019, 12, 118-125.	3.4	13
213	Multiwindow SRS Imaging Using a Rapid Widely Tunable Fiber Laser. Analytical Chemistry, 2021, 93, 15703-15711.	6.5	13
214	Highâ€speed intraâ€operative assessment of breast tumour margins by multimodal ultrasound and photoacoustic tomography. Medical Devices & Sensors, 2018, 1, e10018.	2.7	12
215	Photoinactivation of Catalase Sensitizes <i>Candida albicans</i> and <i>Candida auris</i> to ROSâ€Producing Agents and Immune Cells. Advanced Science, 2022, 9, e2104384.	11.2	12
216	Imaging Cytoplasmic Lipid Droplets in Enterocytes and Assessing Dietary Fat Absorption. Methods in Cell Biology, 2013, 116, 151-166.	1.1	11

#	Article	IF	CITATIONS
217	Photoinactivation of catalase sensitizes a wide range of bacteria to ROS-producing agents and immune cells. JCI Insight, 2022, 7, .	5.0	10
218	Electronic Preresonance Stimulated Raman Scattering Imaging of Red-Shifted Proteorhodopsins: Toward Quantitation of the Membrane Potential. Journal of Physical Chemistry Letters, 2019, 10, 4374-4381.	4.6	9
219	Highly sensitive lipid detection and localization in atherosclerotic plaque with a dualâ€frequency intravascular photoacoustic/ultrasound catheter. Translational Biophotonics, 2020, 2, e202000004.	2.7	9
220	Plasmon-enhanced coherent anti-stokes Raman scattering vs plasmon-enhanced stimulated Raman scattering: Comparison of line shape and enhancement factor. Journal of Chemical Physics, 2021, 154, 034201.	3.0	9
221	Granadaene Photobleaching Reduces the Virulence and Increases Antimicrobial Susceptibility of <i>Streptococcus agalactiae</i> . Photochemistry and Photobiology, 2021, 97, 816-825.	2.5	9
222	Quantitative imaging of intraerythrocytic hemozoin by transient absorption microscopy. Journal of Biomedical Optics, 2019, 25, 1.	2.6	9
223	New imaging techniques in the diagnosis of multiple sclerosis. Expert Opinion on Medical Diagnostics, 2008, 2, 1055-65.	1.6	9
224	Coherent Raman scattering imaging with a near-infrared achromatic metalens. APL Photonics, 2021, 6, 096107.	5.7	8
225	Cylindrical illumination with angular coupling for whole-prostate photoacoustic tomography. Biomedical Optics Express, 2019, 10, 1405.	2.9	8
226	Stimulated Raman scattering signal generation in a scattering medium using self-reconstructing Bessel beams. Photonics Research, 2020, 8, 929.	7.0	7
227	Wide-Field Surface-Enhanced Coherent Anti-Stokes Raman Scattering Microscopy. ACS Photonics, 2022, 9, 1042-1049.	6.6	7
228	Coherent anti-Stokes Raman scattering imaging under ambient light. Optics Letters, 2016, 41, 3880.	3.3	6
229	Nanoladders Facilitate Directional Axonal Outgrowth and Regeneration. ACS Biomaterials Science and Engineering, 2018, 4, 1037-1045.	5.2	6
230	Bond-selective interferometric scattering microscopy. Journal Physics D: Applied Physics, 2021, 54, 364002.	2.8	6
231	Origin of dispersive line shapes in plasmon-enhanced stimulated Raman scatteringÂmicroscopy. Nanophotonics, 2020, 10, 617-625.	6.0	6
232	Chemical imaging of fresh vascular smooth muscle cell response by epiâ€detected stimulated Raman scattering. Journal of Biophotonics, 2018, 11, e201700005.	2.3	5
233	Imaging of demineralized enamel in intact tooth by epidetected stimulated Raman scattering microscopy. Journal of Biomedical Optics, 2018, 23, 1.	2.6	5
234	High-precision neural stimulation through optoacoustic emitters. Neurophotonics, 2022, 9, 032207.	3.3	5

#	Article	IF	CITATIONS
235	NON-LINEAR OPTICAL IMAGING OF OBESITY-RELATED HEALTH RISKS: REVIEW. Journal of Innovative Optical Health Sciences, 2009, 02, 9-25.	1.0	4
236	Room-Temperature Phosphorescence and Low-Energy Induced Direct Triplet Excitation of Alq <sub>3</sub> Engineered Crystals. Journal of Physical Chemistry Letters, 2020, 11, 9364-9370.	4.6	4
237	Intravascular Photoacoustic Imaging of Lipid-Laden Plaques: From Fundamental Concept Toward Clinical Translation. , 2020, , 81-104.		4
238	Label-Free Stimulated Raman Scattering Imaging of Neuronal Membrane Potential. , 2019, , 107-122.		3
239	Ligand-functionalized gold nanorods as theragnostic agents. , 2009, , .		2
240	Converting Molecular Vibration to Mechanical Wave for Bond-Selective Imaging of Deep Tissue. Chinese Journal of Chemical Physics, 2015, 28, 375-382.	1.3	2
241	Assessing carotid atherosclerosis by fiber-optic multispectral photoacoustic tomography. Proceedings of SPIE, 2015, , .	0.8	2
242	Real-time imaging of surface chemical reactions by electrochemical photothermal reflectance microscopy. Chemical Science, 2021, 12, 1930-1936.	7.4	2
243	Pre-resonance stimulated Raman scattering spectroscopy and imaging of membrane potential using near-infrared rhodopsins. , 2019, , .		2
244	Coherent anti-Stokes Raman scattering microscopy. , 2008, , .		1
245	Coupling CARS with multiphoton fluorescence and high harmonic generation imaging modalities using a femtosecond laser source. Proceedings of SPIE, 2009, , .	0.8	1
246	Imaging of Myelin by Coherent Anti-Stokes Raman Scattering Microscopy. Springer Protocols, 2012, , 281-291.	0.3	1
247	Real-time intravascular photoacoustic-ultrasound imaging of lipid-laden plaque at speed of video-rate level. Proceedings of SPIE, 2017, , .	0.8	1
248	NEW ADVANCES IN COHERENT ANTI-STOKES RAMAN SCATTERING (CARS) MICROSCOPY. , 2002, , .		1
249	Fenofibrate (FEN), a peroxisome proliferator activated receptor alpha (PPAR α) agonist, decreases dietary fat absorption and alters triglyceride (TG) metabolism in enterocytes of mice. FASEB Journal, 2010, 24, 210.1.	0.5	1
250	Labelâ€free Spectroscopic Imaging of Lipids in Live Cells and Intact Tissues. FASEB Journal, 2013, 27, 813.6.	0.5	1
251	Rapid Antimicrobial Susceptibility Testing by Stimulated Raman Scattering Imaging of Deuterium Incorporation in a Single Bacterium. Journal of Visualized Experiments, 2022, , .	0.3	1
252	Abstract 253: Vibrational Photoacoustic Imaging of Lipid in Murine Abdominal Aortic Aneurysms and Atherosclerosis. Arteriosclerosis, Thrombosis, and Vascular Biology, 2015, 35, .	2.4	1

#	Article	IF	CITATIONS
253	New "HOPE―laser for photoacoustic imaging of water. Light: Science and Applications, 2022, 11, 107.	16.6	1
254	Biomedical and biophysical applications of coherent anti-Stokes Raman scattering microscopy. , 2006, ,		0
255	Coherent anti-Stokes Raman scattering imaging with photonic crytal fiber delivered laser source. , 2006, , .		0
256	Molecular Imaging of Central Nervous System with Multi-modal Nonlinear Optical Microscopy. , 2007, , .		0
257	Multimodality Nonlinear Optical Imaging. , 2008, , .		0
258	New advances of nonlinear optical microscopy. , 2008, , .		0
259	Inside Cover: Bright Three-Photon Luminescence from Gold/Silver Alloyed Nanostructures for Bioimaging with Negligible Photothermal Toxicity (Angew. Chem. Int. Ed. 20/2010). Angewandte Chemie - International Edition, 2010, 49, 3392-3392.	13.8	0
260	Study of Myelin Sheaths by Cars Microscopy. , 2012, , 221-245.		0
261	One platform, multiple insights. Journal of Biophotonics, 2012, 5, 385-386.	2.3	0
262	Stimulated Raman spectroscopic imaging by microsecond delay-line tuning. , 2017, , .		0
263	Antibiotic Resistance: Photoâ€Disassembly of Membrane Microdomains Revives Conventional Antibiotics against MRSA (Adv. Sci. 6/2020). Advanced Science, 2020, 7, 2070035.	11.2	0
264	Association of PAT proteins with cytoplasmic lipid droplets in mouse enterocytes. FASEB Journal, 2009, 23, 343.1.	0.5	0
265	Intestine specific overâ€expression of DGAT1 in mice alters triacylglycerol storage in enterocytes, but not body weight in response to a high fat diet. FASEB Journal, 2009, 23, .	0.5	Ο
266	Singleâ€cell Molecular Profiling of Adipogenesis on an Integrated CARSâ€Confocal Raman Platform. FASEB Journal, 2009, 23, 681.3.	0.5	0
267	Intestine specific expression of DGAT1 reverses the resistance to dietâ€induced obesity phenotype of DGAT1â€deficient female mice. FASEB Journal, 2009, 23, 721.4.	0.5	0
268	Differential roles of acyl oA:diacylglycerol acyltransferase1 (DGAT1) and DGAT2 in dietary fat absorption FASEB Journal, 2011, 25, 105.2.	0.5	0
269	Adipose tissue triglyceride lipase mRNA is present in the small intestine and increased in response to acute and chronic high fat feeding in mice. FASEB Journal, 2011, 25, 936.4.	0.5	0
270	Highly Sensitive Intravascular Photoacoustic Imaging with a Collinear Catheter Probe. , 2016, , .		0

#	Article	IF	CITATIONS
271	Absorption-Based Far-Field Label-Free Super-Resolution Microscopy. Biological and Medical Physics Series, 2019, , 137-169.	0.4	0
272	SRS image cytometry for high-content single cell analysis. , 2019, , .		0
273	40â€3: Invited Paper: A Large RGBâ€echromatic Metalens for Virtual/Augmented Reality Applications. Digest of Technical Papers SID International Symposium, 2020, 51, 575-578.	0.3	0
274	Investigating antibiotics in cells with pre-resonance stimulated Raman scattering hyperspectral microscopy. , 2021, , .		0
275	Converting hyperspectral SRS into chemical maps. , 2022, , 359-369.		0
276	Rapid determination of antimicrobial susceptibility by SRS single-cell metabolic imaging. , 2022, , 445-461.		0
277	Resolving molecular orientation by polarization-sensitive stimulated Raman scattering microscopy. , 2022, , 529-537.		0
278	Plasmon-enhanced stimulated Raman scattering microscopy. , 2022, , 343-356.		0
279	Miniaturized handheld stimulated Raman scattering microscope. , 2022, , 551-560.		0
280	Multiplex stimulated Raman scattering microscopy via a tuned amplifier. , 2022, , 91-98.		0
281	Deep Brain Optoacoustic Stimulation Enabled by a Multifunctional Fiber-based Optoacoustic Emitter. ,		0